12-1-2021

Unusual Intraclast Conglomerates in a Stormy, Hot-House Lake: The Early Triassic North China Basin

Kaixuan Ji
China University of Geosciences

Paul B. Wignall
University of Leeds

Jeff Peakall
University of Leeds

Jinnan Tong
China University of Geosciences

Daoliang Chu
China University of Geosciences

See next page for additional authors

Recommended Citation

Authors

Kaixuan Ji, Paul B. Wignall, Jeff Peakall, Jinnan Tong, Daoliang Chu, and Sara B. Pruss

Unusual intraclast conglomerates in a stormy, hot-house lake: The Early Triassic North China Basin

KAIXUAN JI*,† , PAUL B. WIGNALL†, JEFF PEAKALL† , JINNAN TONG*,
DAOLIANG CHU* and SARA B. PRUSS‡

*State Key Laboratory of Biogeology and Environmental Geology, School of Earth Science, China University of Geosciences, Wuhan, 430074, China (E-mail: jntong@cug.edu.cn)
†School of Earth and Environment, University of Leeds, Leeds, LS2 9JT, UK
‡Department of Geosciences, Smith College, Northampton, MA, 01063, USA

Associate Editor – Christopher Fielding

ABSTRACT

Early Triassic temperatures were some of the hottest of the Phanerozoic, sea-surface temperatures approached 40°C, with profound consequences for both the sedimentology and faunal distributions in the oceans. However, the impact of these temperatures in terrestrial settings is unclear. This study examines shallow lacustrine sediments from the Lower Triassic succession of North China. These consist of diverse fluvial to shallow lacustrine sandstones and also spectacular, coarse conglomerates composed of diverse, intraformational clasts reworked from the interbedded sediments. The conglomerate beds can show inverse grading and high angle, flat-pebble imbrication in their lower part and vertically orientated flat pebbles in their upper part. The cobbles include cemented and reworked conglomerate intraclasts and sandstone concentrically-laminated concretions that record multi-step histories of growth and reworking, pointing to rapid cementation of the sandy lake bed (likely facilitated by high temperatures). The conglomerates record frequent, high-energy events that were capable of brecciating a lithified lake bed and transporting cobbles in wave-influenced sediment-gravity flows. Initially, powerful oscillatory flows brecciated and deflated the lake bed and subsequently helped to sustain turbulence during short-distance lateral flow. It is possible that hurricanes, originating from the adjacent hyper-warm, Palaeo-Tethyan Ocean travelled into the major lakes of the North China continent during the Early Triassic.

Keywords Conglomerates, early Triassic, North China, storms, terrestrial.

INTRODUCTION

The Permo–Triassic mass extinction coincided with rapid warming that culminated with equatorial sea-surface temperatures which were by far the hottest of the Phanerozoic; approaching 40°C in the later Early Triassic (Sun *et al.*, 2012). This Permo–Triassic thermal maximum made life in equatorial settings difficult and was a major factor in the development of widespread ocean anoxia (Wignall, 2015). These

conditions also lead to frequent seafloor lithification in carbonate settings (Wignall & Twitchett, 1999; Woods *et al.*, 2007), abundant ooid production (Li *et al.*, 2019) and microbialite growth (Pruss *et al.*, 2005; Baud *et al.*, 2007). The impact of extreme warmth on marine environments is therefore well-known. The effect on terrestrial life was manifest in that tetrapods became extremely rare in equatorial climes, probably due to the difficulties of sustaining their high metabolic lifestyles at excessively

high temperatures (Sun *et al.*, 2012; Allen *et al.*, 2020; Romano *et al.*, 2020). However, the effect of high temperatures on Early Triassic terrestrial sedimentation is less understood. It has been proposed that there may have been a major increase of aridity, for example, in North China, which was situated at low northern palaeolatitudes (Romano *et al.*, 2020; Zhu *et al.*, 2020), and in the Karoo Basin at high southern palaeolatitudes (Smith & Botha-Brink, 2014; MacLeod *et al.*, 2017). Strong seasonality is another notable feature at both low northern (for example, South China) (Chu *et al.*, 2020) and high southern palaeolatitudes (for example, Sydney Basin) (Fielding *et al.*, 2019). Lakes provide especially good records of prevailing continental climate, and this study examines an Early Triassic fluvial–lacustrine system from the Liujiagou Formation of North China, focussing on the origin of some highly unusual intraclast conglomerates which are interpreted to be the product of the exceptional climatic conditions of the Early Triassic.

REGIONAL GEOLOGY

A series of large, intracontinental basins developed in northern China during the Permian and Triassic on a stable, cratonic foreland (for example, the Junggar and Ordos basins) and were infilled with a range of continental facies: lacustrine, deltaic, fluvial and alluvial fan (Liu *et al.*, 2015). The North China basins occupied central, northern China and during the Early Triassic they were located at low, temperate latitudes (25–30°N) (Liu *et al.*, 2015; Torsvik & Cocks, 2016) (Fig. 1). During lacustrine intervals alluvial facies fringed a lake within the Basin and, at times, alluvial conditions extended across the entire region (Zhu *et al.*, 2020).

The Permo–Triassic stratigraphy of the studied sections belongs to the Shiqianfeng Group which is divided, in stratigraphic order, into the Sunjiagou, Liujiagou and Heshanggou formations. The lower part of the Sunjiagou Formation contains the *Ullmania bronni–Yuania magnifolia* plant fossil assemblage, the youngest Permian flora known from the region (Wang & Wang, 1986). Based on fossil content, the Permo–Triassic boundary is placed in the uppermost part of the Sunjiagou Formation whilst the base of the Spathian Substage approximately coincides with the base of the Heshanggou

Formation (Tu *et al.*, 2016), indicating that the intervening Liujiagou Formation encompasses the Griesbachian to Smithian substages.

The Sunjiagou Formation ranges from 76 to 106 m thick, and consists of fine-grained sandstones, siltstones and mudstones interpreted to have formed mostly in terrestrial conditions although the presence of marine fossils in the south-west of the basin, suggests that the ocean lay in this direction and was, at times, in open connection with the North China Basin. In contrast to the Sunjiagou Formation, the Liujiagou Formation is overwhelmingly dominated by fine to medium-grained sandstone. The basal contact is sharp and likely to represent an unconformity/sequence boundary (Zhu *et al.*, 2020). Thicknesses of the Liujiagou Formation range from 111 to 340 m, and increase gradually from the south-west to the north-east in the North China Basin. Reported sedimentary features include cross-bedding, planar lamination, desiccation cracks, wave and current ripples, and wrinkle marks attributed to microbial mats (Chu *et al.*, 2017; Chu *et al.*, 2019). The depositional environments of the Liujiagou Formation are debated, although there is a consensus that braided, fluvial facies are important (Chu *et al.*, 2015; Tu *et al.*, 2016; Zhu *et al.*, 2020). Shallow lacustrine facies, with fringing fluviodeltaic facies, are also present as evidenced by the wave ripples and wrinkle marks (Chu *et al.*, 2015; Tu *et al.*, 2016). Zhu *et al.* (2020) also identified such facies, but considered aeolian facies to be more important. However, their two study sections in northern Shanxi Province were situated at the northern edge of the Basin and, as documented below, there is considerable evidence for subaqueous deposition over large areas of the Basin which rather suggests that the region did not experience an arid climate in the Early Triassic. Within this debated depositional context, this paper reports the presence of unusual, near-surface concretion growth and intraformational conglomerate formation. The succeeding Heshanggou Formation consists of red mudstones and subordinate sandstones ascribed to fluvial, floodplain and lacustrine origins (Guo *et al.*, 2019; Zhu *et al.*, 2020).

STUDY AREA AND TECHNIQUES

Detailed sedimentary logging was undertaken at four main study sites (Figs 1 and 2), and
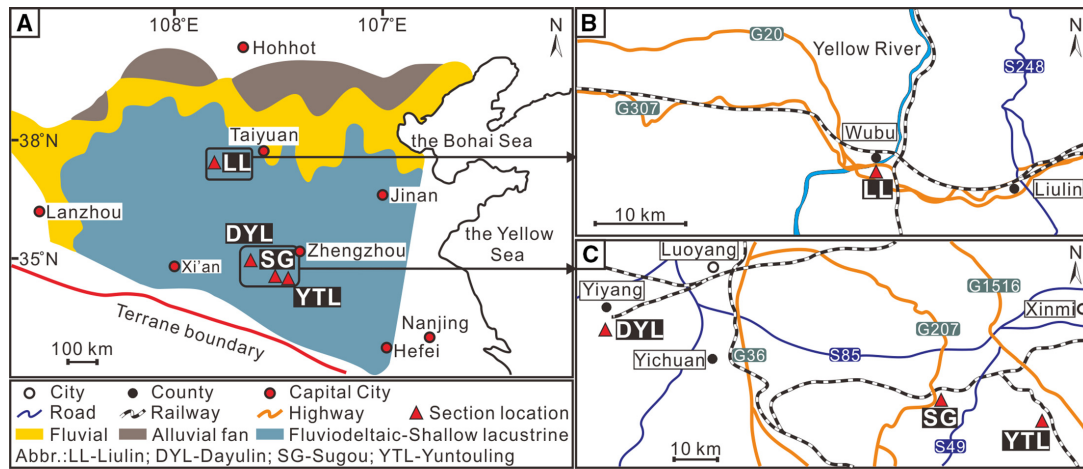
Fig. 1. Early Triassic regional palaeogeography of North China (A) and location map of study sections (B) and (C).

palaeocurrents measured, with 63 samples taken for petrographic analysis. Where closely spaced outcrops were available, correlation panels were constructed to assess lateral variation of beds. Detailed sketches were also made of clast orientations, on vertical and horizontal faces, within the numerous conglomerate beds that were encountered.

Three sections of the Liujiagou Formation were studied in Henan Province:

Yuntouling (34°17'33"N, 113°14'53"E), located in Yuzhou city, where a 50 m thick section of the Liujiagou Formation was examined amongst frequent small, somewhat discontinuous outcrops of light grey to red sandstone and conglomerate beds exposed along a hillside.

Sugou (34°20'4"N, 112°59'17"E) located in Dengfeng City, 25 km west of Yuntouling. Continuous but slightly discontinuous outcrops occur along a wooded hillside.

Dayulin (34°30'6"N, 112°9'20"E), in Yiyang County is an important reference section in Henan Province, 80 km west of Sugou section. The outcrops consist of a large roadcut, that provides a continuous exposure of the Sunjiagou Formation, whilst an adjacent creek section provides extensive exposures of the Liujiagou Formation.

A fourth section, at *Liulin* (37°28'6"N, 110°40'60"E), in Shanxi Province, provides a long continuous section (more than 500 m thick) from the Sunjiagou to the Heshanggou formations along a roadcut adjacent to the Yellow River (Fig. 2). This location is about 440 km north of Dayulin section (Fig. 1).

FACIES DESCRIPTIONS

The Liujiagou Formation records a range of depositional conditions, with fluvial facies being especially prevalent, together with potential aeolian facies (Zhu *et al.*, 2020). Here, observations are restricted to the lacustrine and lake-margin facies that include conglomerates that form the focus of the study.

Mudstone facies

This facies consists of red mudstone beds ranging from 1 to 30 cm thick. They are typically massive, but can also show weak bedding and occasionally thin sandstone laminae up to 5 mm thick. The mudstone facies is a relatively minor constituent of the Liujiagou Formation and is best developed at Liulin.

Cross-bedded sandstone facies

This facies is the most common in the Liujiagou Formation and consists of red medium-grained sandstones with trough cross-bedding or, more rarely, tabular cross-sets. Set thickness ranges from 0.1 m up to 1.0 m and can either consist of isolated sets or stacked cosets forming packages up to 4 m thick. At Liulin the lamination is often picked out by colour variations that range from deep red to pale pink (Fig. 3A). This stripey appearance resembles the pin-stripe lamination noted by Zhu *et al.* (2020) from other outcrops of the Liujiagou Formation, although there was no grain-size variation associated with
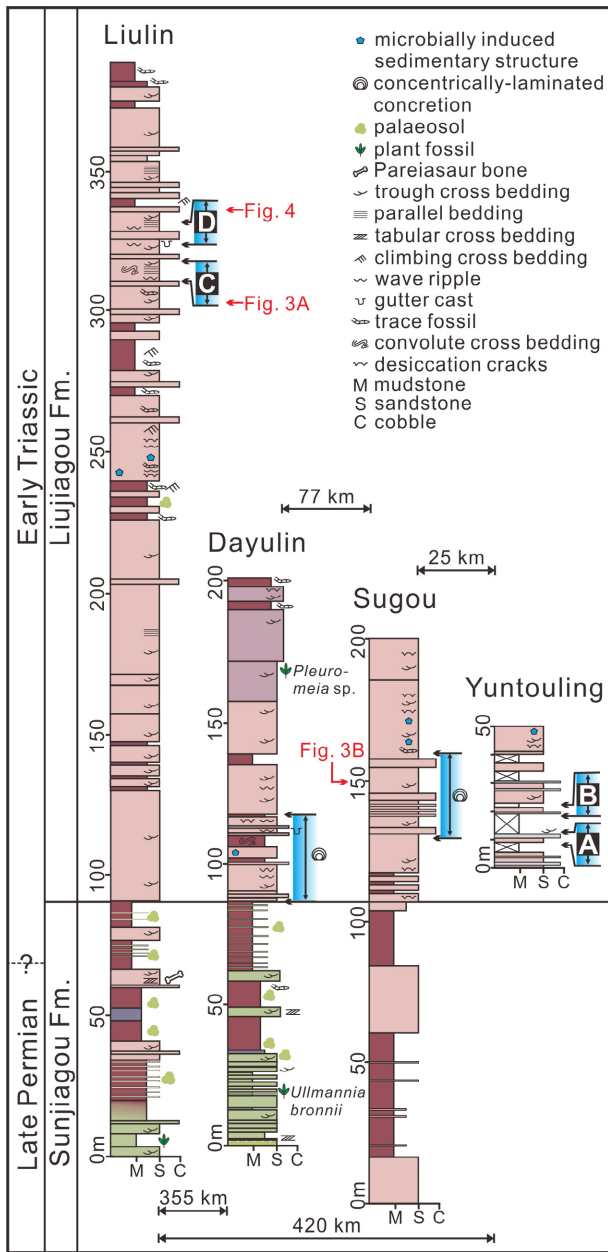
Fig. 2. Summary lithological columns of the Liulin, Dayulin, Sugou and Yuntouling sections. Blue shadows with arrows mark the beds with concentrically-laminated concretions (CLCs). Sedimentary logs at (A), (B), (C) and (D) are shown in Fig. 5.

Fig. 3. (A) Colour-laminated trough cross-bedding of Liujiagou Formation, Liulin Palaeocurrent is from right to left (southward). Wenchao Shu is 1.7 m tall. (B) Multidirectional, trough cross-bedded sandstone of the Liujiagou Formation, Sugou. Height of face is *ca* 1 m. (C) Sketch of cross-bedding in (B). Locations of strata are shown in Fig. 2.

(Fig. 3A) whilst other cosets show great variability (Fig. 3B and C).

Planar-laminated sandstone

Persistent sheets of red planar-laminated medium-grained sandstone are often interbedded with the red mudstone and cross-bedded sandstone facies. The basal portion of beds can have red mud chips when in contact with the mudstone facies. Bedding surfaces often show primary current lineation.

Swaley cross-stratified sandstone facies

This facies is comprised of red and grey-purple, medium-grained sandstone showing broad,

the colour banding. Where the cross-bedded sandstone beds rest on mudstone facies, the contact is often slightly erosive with mud chips (up to 20 cm in diameter) resting on the basal surface in the toesets and also occasionally scattered on the foresets. Cross-bed flow directions vary considerably: some cosets can show a flow
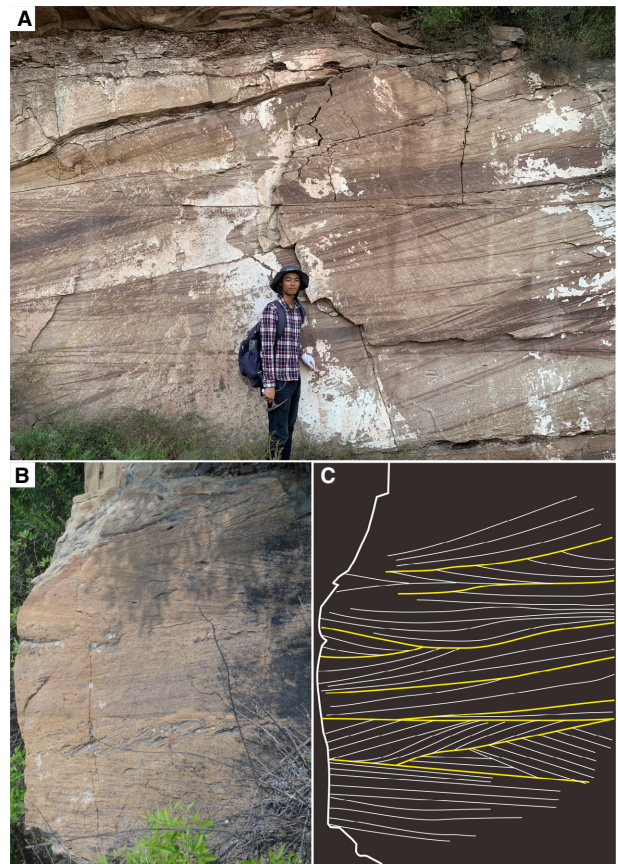
erosive troughs, up to 2 m in diameter and 20 cm deep, with smaller examples typically having half these dimensions. Beds of swaley cross-stratified (SCS) sandstone range from 0.3 to 1.0 m thick. The troughs are infilled with strata that show concave-up (swaley) laminae and in some examples the later part of the trough filling becomes hummocky (Fig. 4B). In a few examples, the flanks of the troughs have mud chips at the basal contact. Occasionally the troughs have not been infilled with sand and are instead filled with red mudstone of the overlying beds.

Wave-rippled sandstone facies

This facies consists of red and grey-purple fine and medium-grained sandstone with wave ripples. Two main types occur, and the first consists of isolated beds of generally small wave ripples (wavelengths *ca* 2 to 3 cm) (e.g. Chu *et al.*, 2017, fig. 2F). This type is often associated with wrinkle structures, and likely produced microbial mats, such as the 'old elephant skin' textures described by Chu *et al.* (2017). The second type comprises beds up to 0.5 m thick of aggrading wave ripples with larger
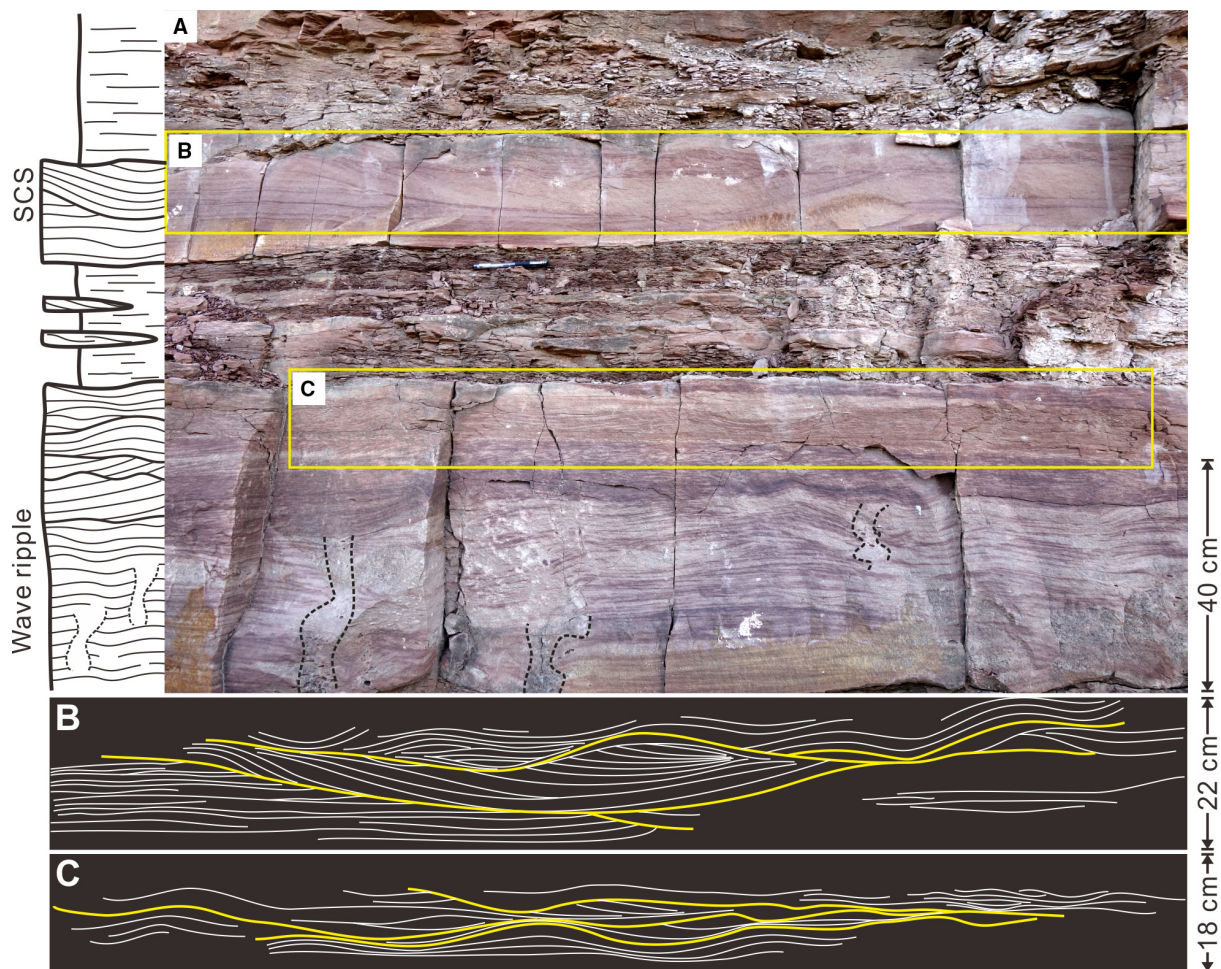

Fig. 4. Strata in the Liulin section. (A) Interbedded red sandstone and mudstone beds with bedding styles shown in panels (B) and (C). Irregular, near-vertical zones of homogenous sediment, marked with black dashed lines in the lower part of the face are interpreted as burrows, likely escape traces. (B) shows scours with swaley cross-stratification (SCS) fill that locally grades into hummocky cross-stratification and (C) shows aggrading wave-rippled horizons. Location of outcrop is shown in Fig. 2.

wavelengths (Fig. 4C). Occasional examples of *Skolithos* cut the aggrading wave ripple laminae, as do irregular, vertical zones of disruption, approximately 5 cm wide. The latter often terminate in a broad funnel within the aggrading wave ripple beds and are considered to be a form of escape trace (Fig. 4A).

Intraformational conglomerate facies

This facies consists of red and grey conglomeratic beds with intraformational clasts spanning a broad range of sizes from a few millimetres up to 30 cm in diameter. The diverse types and origins of the clasts are described and discussed below.

Beds range from 0.2 to 1.0 m thick and contacts are invariably sharp and erosive, showing up to several decimetres of erosive relief. Where beds can be traced laterally they often show both bed cut-out and amalgamation (Fig. 5A and B). Gutters, seen at basal contacts, can be aligned at high angles to the prevailing flow direction recorded by the cross-bedding described below (Fig. 6).

Generally, the clasts in the intraformational conglomerate facies generally do not show well-developed grading, although weak inverse grading is sometimes seen in the basal parts of beds, and the largest clasts are often found within the centre of the beds. Occasionally the conglomerate beds pass upward into either

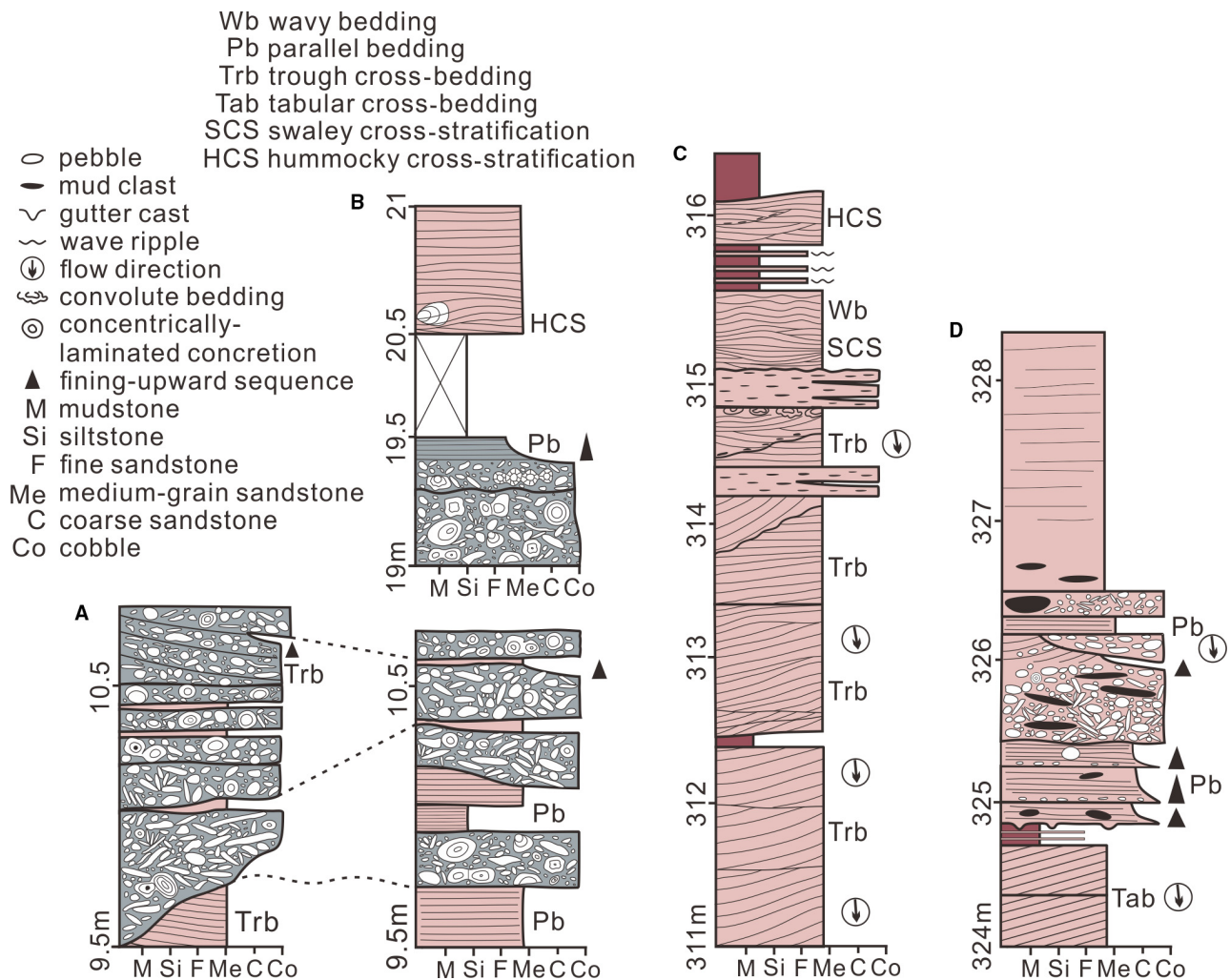**Fig. 5.** Sedimentary logs of the Liujiagou Formation. (A) and (B) intraclast conglomerate beds with reworked concretions, Yuntouling. Location (A) shows correlation of two short sections *ca* 15 m apart, revealing the lateral impersistence/amalgamation of the conglomeratic horizons and their erosive basal contacts. (C) and (D) Cross-bedded sands capped by an intraformational conglomerate, Duizuiya.
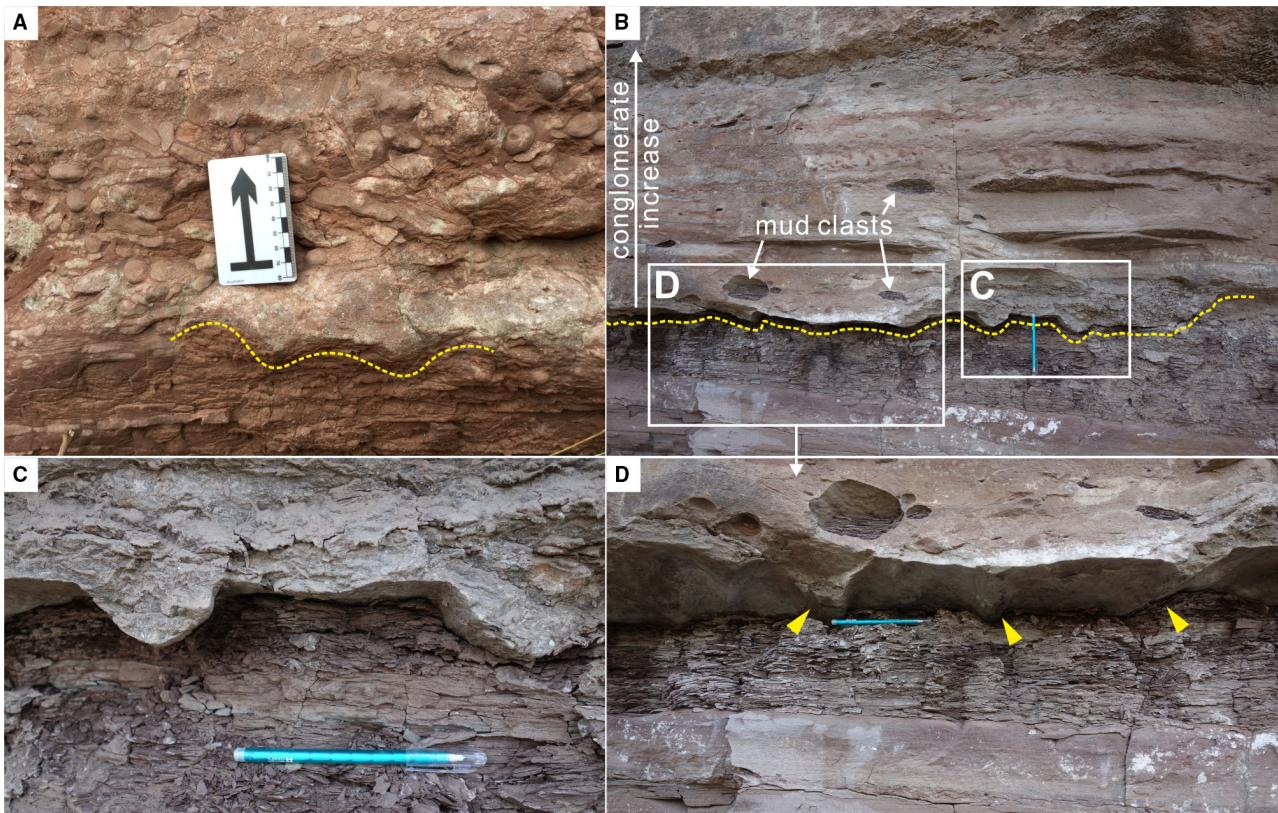
Fig. 6. Gutter casts from Dayulin (A) and Liulin (B) to (D). (A) Gutter casts, emphasized with yellow dashed line, at the base of an intraformational conglomerate beds, that are aligned orthogonally to the flow direction recorded by imbrication in the overlying strata. (B) Erosion surface with several gutter casts. The conglomeratic component of the bed includes mudstone boulders, especially in the lower part of the bed where they have been partially lost due to modern erosion leaving hollows in the outcrop. (C) and (D) show details of the gutter casts (yellow arrows) in (B). Pencil for scale is 14 cm long.

planar-laminated or trough cross-stratified medium-grained sandstones. Some examples of conglomerate beds show low angle cross-sets, with foresets distinguished by changes in the average grain size of clasts (Fig. 5A). Clast shape is varied and ranges from angular to spherical blocks and includes common flat pebbles up to 10 cm in maximum dimension (Fig. 7). The latter often show no preferred orientation, especially in the centre of beds, but they can also occur in alignment. Towards the base of beds (but not at the base), the flat pebbles can show imbricate stacking, often at angles of *ca* 30° and sometimes higher (Fig. 7D and G), especially where the flat pebbles have lodged in the spaces between larger clasts. Where visible, this alignment shows that the long axis (a-axis) of the clasts are dipping upflow. In the topmost parts of beds, the flat pebbles often show vertical alignment (Fig. 7B

and F) and, occasionally, are arranged in radial fans (Fig. 7C). These latter examples are reminiscent of the 'vertically imbricated rosettes' seen in Cambrian flat-pebble conglomerates (Myrow *et al.*, 2004, fig. 3D), although the Liujiagou examples are untidier.

The matrix of intraformational conglomerates includes sand-grade material, coarse sparry calcite cement and pyrite crystals. Within individual beds the matrix is usually concentrated in the lower part with cement dominating in the upper part (Fig. 7). Areas of shelter porosity are common where larger clasts, typically flat pebbles, have roofed a void beneath which finer sediment is absent (Fig. 8A). This observation strongly suggests that the matrix sediment infiltrated downward into the pebble piles after their emplacement. Narrow zones of isopachous fringe cement are developed on some intraclasts but coarse, poikilotopic, sparry
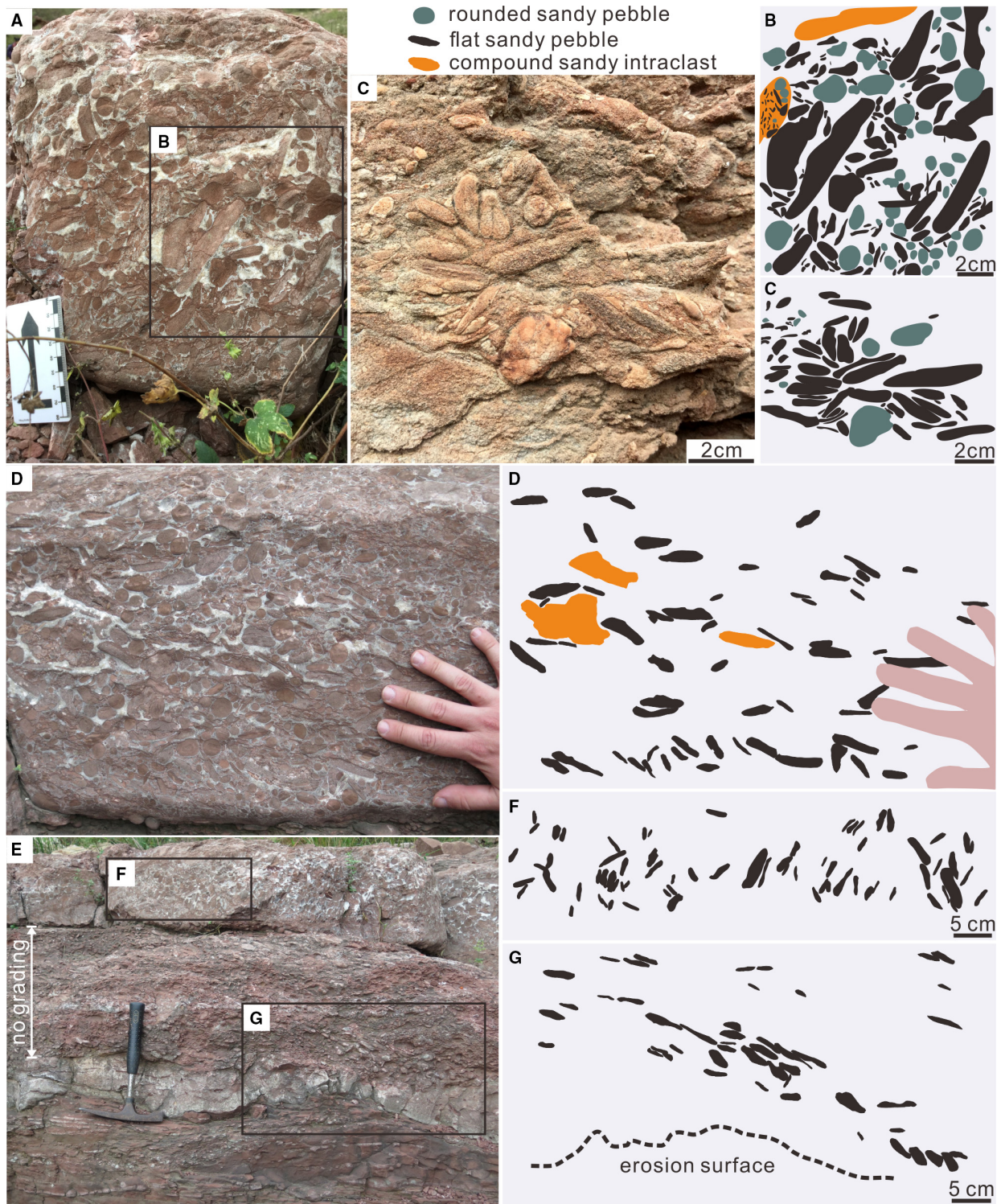
Fig. 7. Photographs and interpretive sketches of flat pebbles seen in vertical views. All from Dayulin except (C) which is from Liulin. (A) and (B) show the dominance of high angles amongst the largest clasts. (C) Shows a fan-like structure developed in a flat-pebble conglomerate. (D) Imbricated flat pebbles from near the bottom of a conglomerate bed that shows inverse grading. (E) Intraclast conglomerate bed with variable stacking of flat pebbles. Note that cementation of the basal *ca* 15 cm of the bed has somewhat obscured the clasts at this level. Hammer for scale is 40 cm long. (F) Vertical alignment of flat pebbles in the topmost parts of bed. (G) High angle imbricated stacking of flat pebbles at the bottom of the bed. For clarity, only flat pebbles and compound intraclasts (reworked conglomerate) are highlighted in interpretive sketches.

cement is the most important void-filling component. The coarse spar has quartz silt grains floating within the cement indicating that cementation was occurring near the sediment surface where sediment was able to infiltrate (Fig. 8B and C).

SEDIMENTARY ENVIRONMENTS

The diverse facies within the Liujiagou Formation suggest a variety of depositional settings that likely spanned from fluvial to lacustrine conditions. The cross-bedded sandstone facies are the most commonly encountered (for example, Fig. 3A) and suggest the importance of channel deposition either within a fluvial or fluviodeltaic context. The planar-laminated sandstone beds could have formed in similar settings, under higher velocity flow regimes, although their often-extensive nature indicates that a distributary mouth bar setting is also possible. In contrast, the presence of stacked sets of cross-beds, recording multidirectional flow, is more typical of shoreface settings (cf. Schuster & Nutz, 2018) and suggests that lacustrine deposition is also recorded in the Liujiagou Formation. Deposition within such a lake is indicated by the presence of wave-rippled and SCS sandstone facies that record the influence of fair-weather and storm waves.

The mudstone facies record quieter deposition from suspension which again is likely to have been in a lacustrine setting. The presence of sand laminae indicates somewhat coarser clastic influx, perhaps from hyperpycnal flows sourced from distal distributaries. The lack of fossils suggests a mostly azoic lake, although the presence of occasional escape traces (and *Skolithos* burrows) in the wave-rippled sandstone facies indicates the occasional presence of a benthic fauna. Potentially some of the mudstone beds could have formed in a floodplain setting, although diagnostic features such as desiccation cracks, pedogenic structures and plant roots are not present. However, the presence of reworked intraclasts of mudstone within the fluvial (or fluviodeltaic) cross-bedded sandstone implies that a muddy floodplain was developed adjacent to the channels.

Overall, the Liujiagou Formation in our study sites records a depositional setting that included extensive lakes and feeder fluvial systems that supplied sand and mud. The lakes were influenced by fair-weather and storm waves, although the water depth is unlikely to have been great as deep-water lake facies are not known. It was in this setting that the intraformational conglomerate horizons were formed by high-energy events of significant strength. Before discussing their origin, in the context of the depositional environments indicated by the other Liujiagou facies, this study first documents the diversity and origin of the constituent clast types.

INTRACLAST TYPES

The intraformational conglomerates of Liujiagou Formation are composed almost entirely of clasts generated within the depositional environment, whilst extraclasts transported into the depositional setting are extraordinarily rare. Five different varieties of clast (Fig. 9) are present:

Mud clasts

Red mud clasts range from *ca* 0.1 mm up to 15 cm in maximum dimension. They range in shape and are commonly flat pebbles or discs, although some of the smallest examples can be irregular in shape (Fig. 10A). The largest examples tend to be more equidimensional and are typically rounded (Figs 6B, 6D and 9). Lithologically, the mud clasts are identical to the interbedded red mudstone facies, from which they are no doubt derived, and they are especially common in the basal parts of erosive-based sandstone beds that rest on mudstones. Some mud clasts exhibit a rind of calcitic, isopachous fringe cement that often shows abrasion.

The truncated cement lining suggests that there were at least two stages of reworking of some mud clasts: the first eroded the clast from a partly lithified mudstone before burial, followed by growth of a cement lining. A second phase of erosion and abrasion partly removed the fringing cement (Fig. 10A to C).

Sandstone clasts

Intraclasts composed of fine to medium-grained sandstone, cemented by fine microspars, are the most common clast type encountered in the intraformational conglomerate facies. They show a diverse range of shapes although spherical and flat pebble varieties are especially common (Fig. 7). Most clasts are in the size range of *ca*
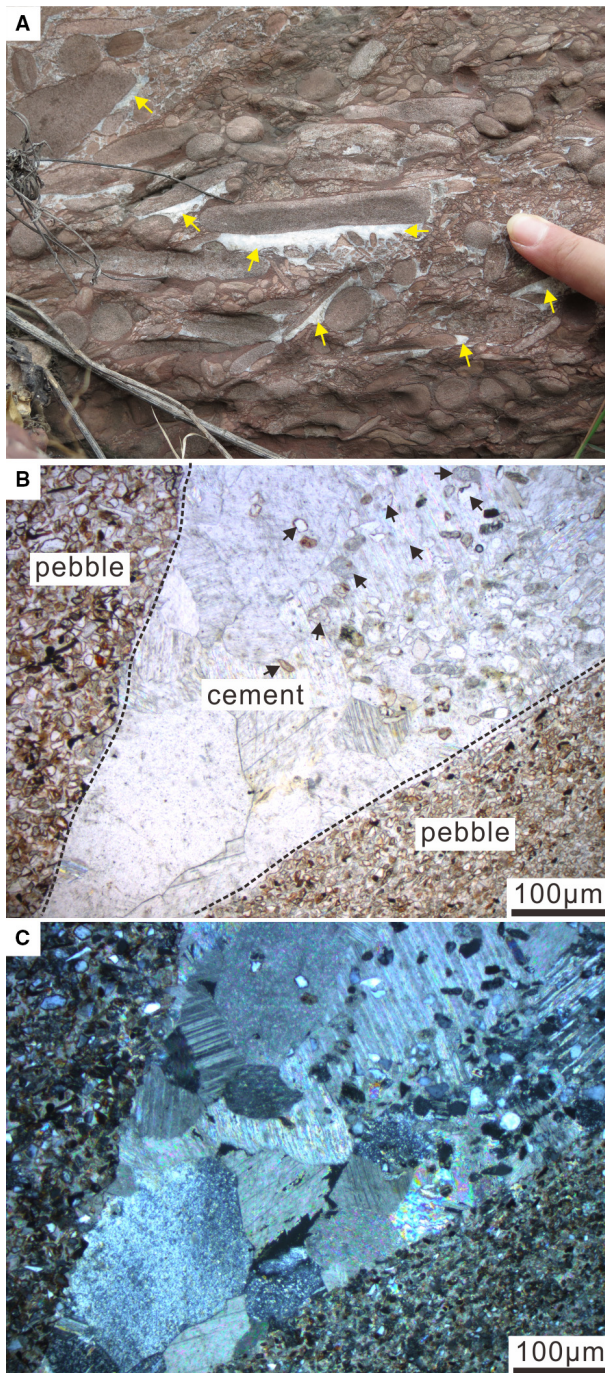
Fig. 8. (A) Conglomerate with shelter porosity infilled with coarse, calcite cement (yellow arrows), Dayulin. (B) and (C) Photomicrographs in plane and cross-polar light showing a calcite cement-filled void developed between two intraclast pebbles. Floating sand grains (black arrows) are seen within the cement, especially in the upper right.

1 mm to 10 cm, but occasionally, some outsized angular clasts can reach 30 cm in maximum dimension (Fig. 11A). It is often possible to see original planar lamination and cross-bedding within the larger clasts.

The sandstone clasts are clearly derived by erosion of the interbedded sandstone facies of the Liujiagou Formation because they are lithologically identical. Rounding of the smaller clasts could be the product of transport and abrasion, although it could also (at least partially) reflect the exhumation of part-cemented spherical and tabular patches of sediment. Examples of spherical concretions of identical size to the spherical clasts seen in the conglomerate facies, are encountered in the interbedded sandstone facies. In contrast, the angular, larger blocks seem to have been derived from fragmentation of more extensively cemented sandstone beds.

Concentrically-laminated concretions

Many sandstone intraclasts are either internally homogenous or show planar lamination but there are also spherical, sandstone clasts that show concentric internal laminae. The concentrically-laminated concretions (CLCs) are present in all of our study sections and they are especially abundant at Yuntouling and Sugou. The clasts range from 3 to 20 cm in diameter, and the laminae are often asymmetrically developed and show a succession of growth phases with later laminae discordant to earlier ones (Fig. 11B and C). The truncation of laminae at the contacts between these phases suggests that periods of abrasion interrupted the growth of the CLCs. In some cases, the final laminae overgrow two (and occasionally three or four, or even six) adjacent CLCs producing large, composite clasts with two spherical core clasts joined to produce a figure '8' pattern in outcrop (Fig. 11D). Examples are also seen whereby the spherical clasts have an attached late stage 'wing' (Fig. 11E) or the concentric laminae have nucleated on sandstone intraclasts (Fig. 11F). Laminae are defined by colour variations from red to pale pink to sandy grey and, in thin section, are defined by subtle variations in the concentration of iron oxides. The CLC cement consists of either microspar or (more rarely) coarse, radially-oriented calcite crystals that are highly reminiscent of the calcite that forms speleothems (Fairchild *et al.*, 2006). Some CLCs show alternations of both types of cement growth (Figs 12A and 13C).

The CLCs are calcite-cemented spheres of sandstone which are considered to be reworked
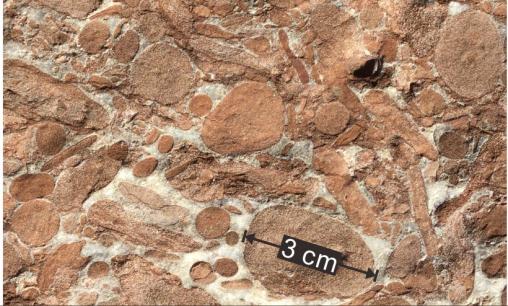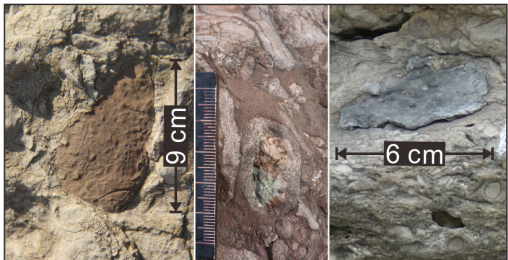
CLAST TYPE	CHARACTERS		REFERENCE
Mud clast			
	colour	dark red	Fig. 6B and D; Fig. 10 A-C
	shape	flat, discs,irregular,rounded	
	size range	0.1 mm−15 cm	
	occurrence	in the basal parts of erosive-based sandstone beds.	
	thin section observation	occasionally show isopachous fringe cement, partly abraded	
Sandstone clasts			
	colour	red, blue-grey	Fig. 7; Fig. 11A
	shape	various, mainly spherical, flat and irregular	
	size range	most are in1 mm−10 cm, some can reach 30 cm in long axis	
	occurrence	the main clast of conglomerate beds	
	thin section observation	calcitic, isopachous fringe cement with abrasions	
Concentrically-laminated concretion			
	colour	red, blue-grey	Fig. 11; Fig. 12; Fig. 14A
	shape	various, mainly in rounded or clusters of several CLCs	
	size range	3−20 cm	
	occurrence	dispersed in conglomerate beds or *in situ* in sandstone	
	thin section observation	isopachous fringe, blocky or radially-oriented calcite cement crystals	
Compound intraclast			
	colour	red, blue-grey	Fig. 7B and D; Fig. 14A
	shape	rounded, irregular, angular	
	size range	2-30 cm	
	occurrence	dispersed in conglomerate beds	
	thin section observation	truncation of internal grains at clast margins	
	composition	mud-chips, sandstone pebbles and calcite cement	
Exotic clasts			
	colour	red, blue-grey, others	Fig. 14B
	shape	various, most are irregular	
	size range	1-20 cm	
	composition	sandstone, micritic limestone and others	
	occurrence	randomly distributed in conglomerate beds	

Fig. 9. Categories of clast found in the Liujiagou Formation, Lower Triassic, North China.
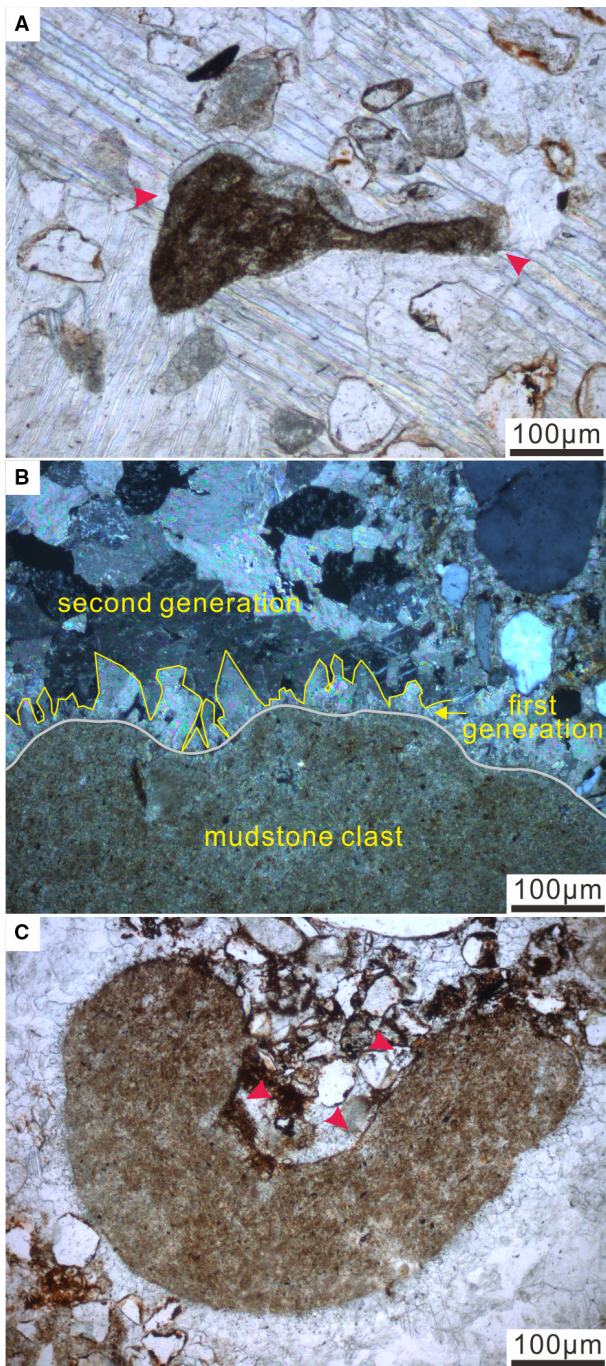
Fig. 10. (A) Mudstone intraclast with fringing isopachous cement that has been partially eroded (arrowed at point of truncation). (B) Mudstone intraclast, with erosion structures, dog-tooth (first generation) and blocky (second generation) calcite cement in the matrix. (C) Silt clast with erosion structures (arrows), bladed (first generation) and blocky (second generation) calcite cement in the matrix.

concretions. This notion is supported by the presence of original bedding within some CLCs (Fig. 12B) and the common occurrence of *in situ* examples in the sandstones interbedded with the conglomerates (Fig. 12C and D). Many of the CLCs have clearly undergone several episodes of reworking. Figure 12 charts the development of some examples that show prolonged, multi-stage histories of formation. Cementation appears to have been close to the sediment surface with the result that the concretions were regularly reworked, reorientated *in situ* (for example, Fig. 13A) or partially exposed on the lake bed and truncated (Fig. 13B). The cement style, from microspar to radial crystals, often varied between reworking episodes (Fig. 13C). Other evidence for early cementation, noted above, includes the abraded, isopachous fringe cement seen on mudstone clasts, floating grains in the coarse spar cement and the presence of conglomerate intraclasts within the conglomerate beds described below.

Compound intraclasts

The conglomerate beds are composed of sandstone and mudstone clasts reworked from the interbedded sediment but there are also clasts of reworked conglomerate of identical lithology (Figs 7B, 7D, 9 and 14A). These compound intraclasts range from rounded to irregular, angular shapes and from a few centimetres to boulders approaching 30 cm in maximum dimension. The truncation of internal grains, such as CLCs, at the margins indicates the reworked/abraded origin of these clasts. Also, the matrix of conglomerate intraclasts can differ from the surrounding sediment. For example, the intraclasts in Fig. 7B have a sandy matrix but are encased in a conglomerate with a sparry calcite matrix.

Exotic clasts

Nearly all the clasts encountered in the conglomerate facies of the Liujiagou Formation were derived from erosion of interbedded sediments. The exceptions are a single pebble of sandstone and rare pebbles of grey–white micritic limestone(s) (Figs 9 and 14B), which range from a few centimetres up to 20 cm in diameter. These lithologies are not seen in the study sections,
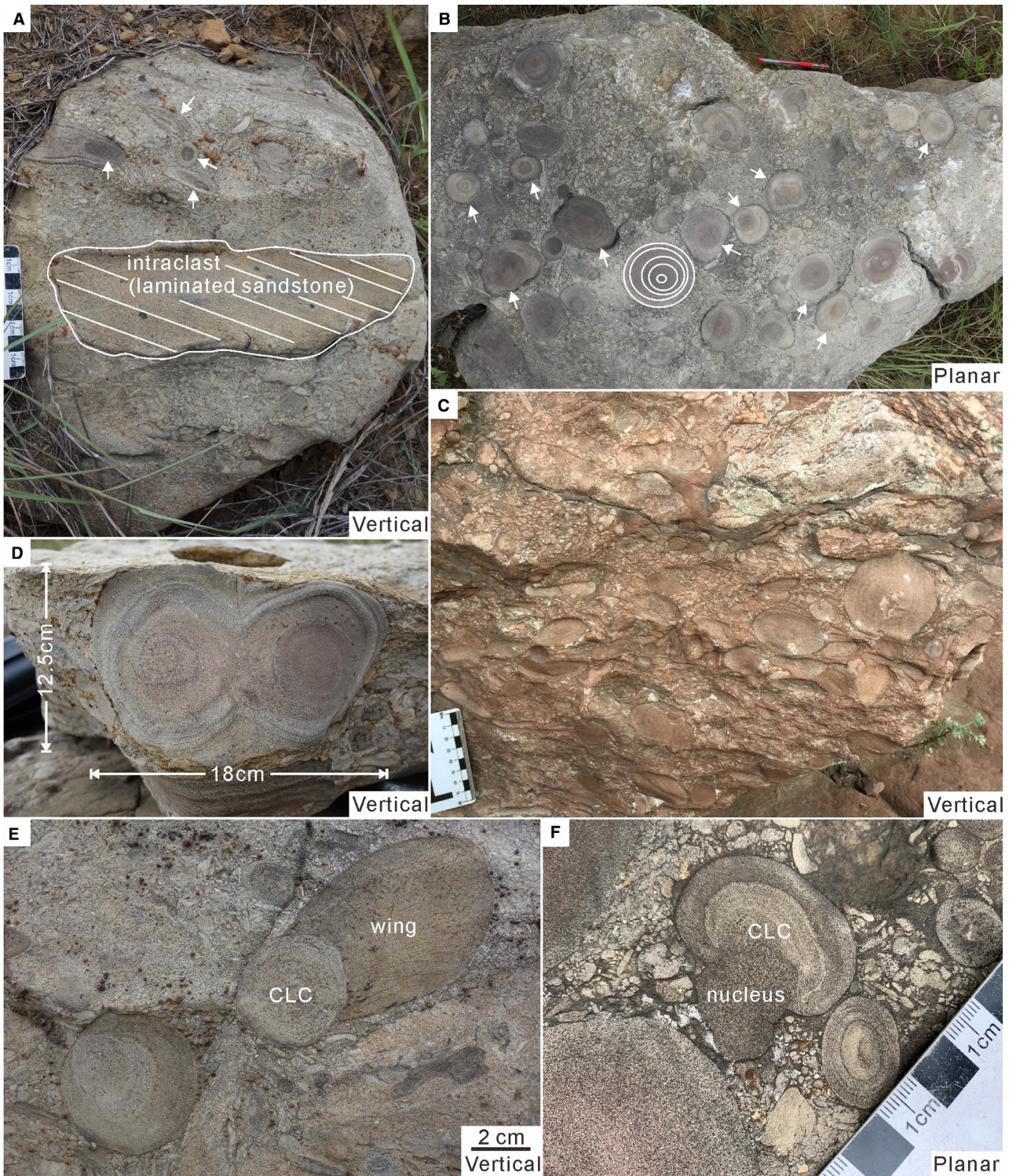
Fig. 11. (A) Intraclast conglomerate with boulder-size sandstone clasts and concentrically-laminated concretions (CLCs; arrowed). (B) Abundant, large CLCs (arrowed and one example highlighted) in a bedding-plane view. Pencil for scale is 14 cm long. (C) Poorly-sorted conglomerate bed showing CLCs and large, conglomerate intraclasts in the upper right. (D) Large clast consisting of two amalgamated CLCs within an intraclast conglomerate bed. (E) CLC with a 'wing' structure – a concretionary overgrowth that shows internal planar lamination. (F) CLC nucleated on a sandstone intraclast. All pictures are from Yuntouling except (C) which is from Dayulin.
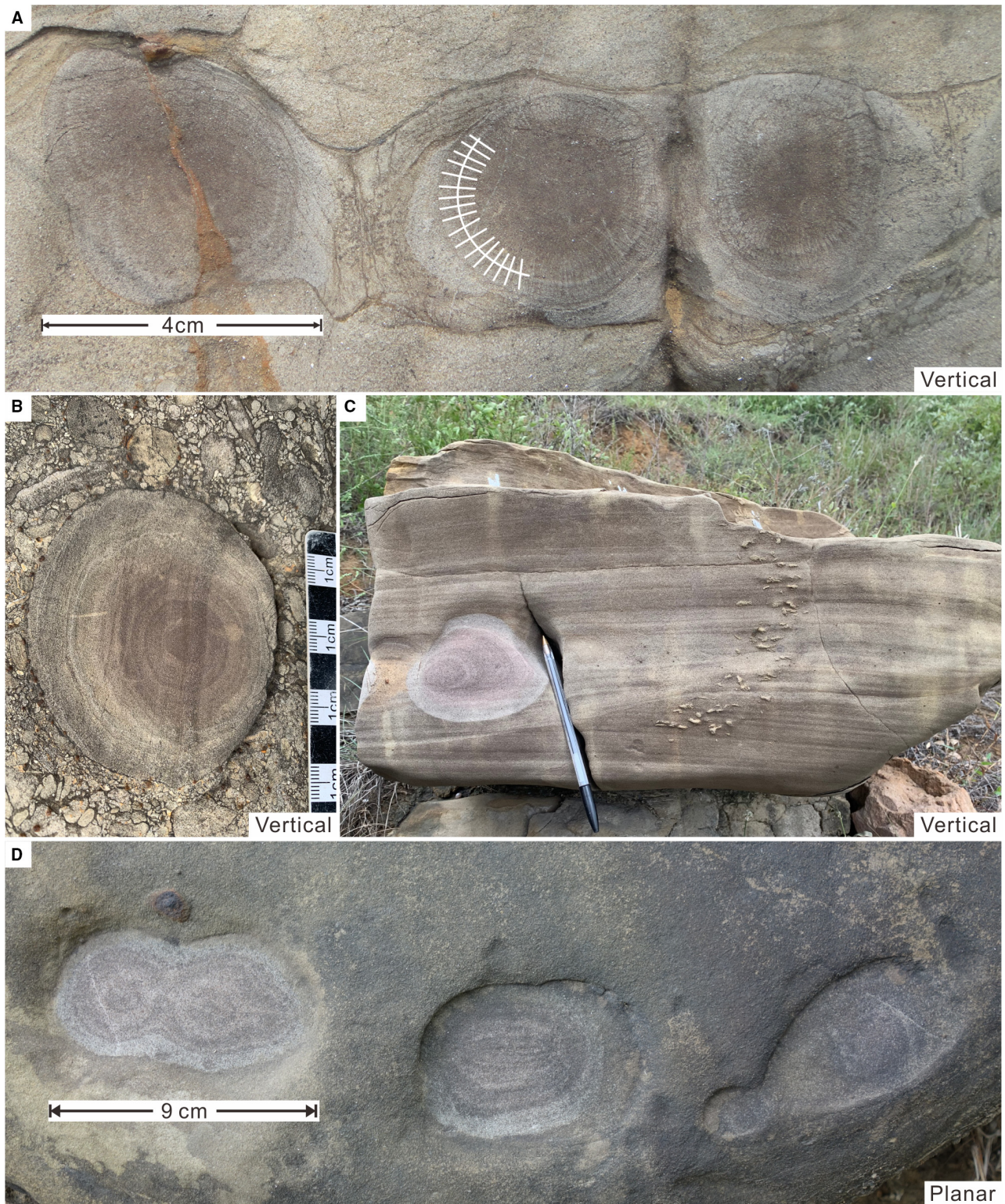
Fig. 12. (A) Three concentrically-laminated concretions (CLCs) showing phases of radially-oriented calcite crystal growth (partially highlighted) on a nucleus with microspar cement. (B) CLC showing planar, internal lamination of the original host sediment and the concentric laminae of the concretionary growth. (C) A laminated sandstone bed with swaley cross-stratification and an unreworked, concentric concretion adjacent to the pen (14 cm long). (D) Sandstone with three CLCs including coalescing examples. All from Yuntouling.
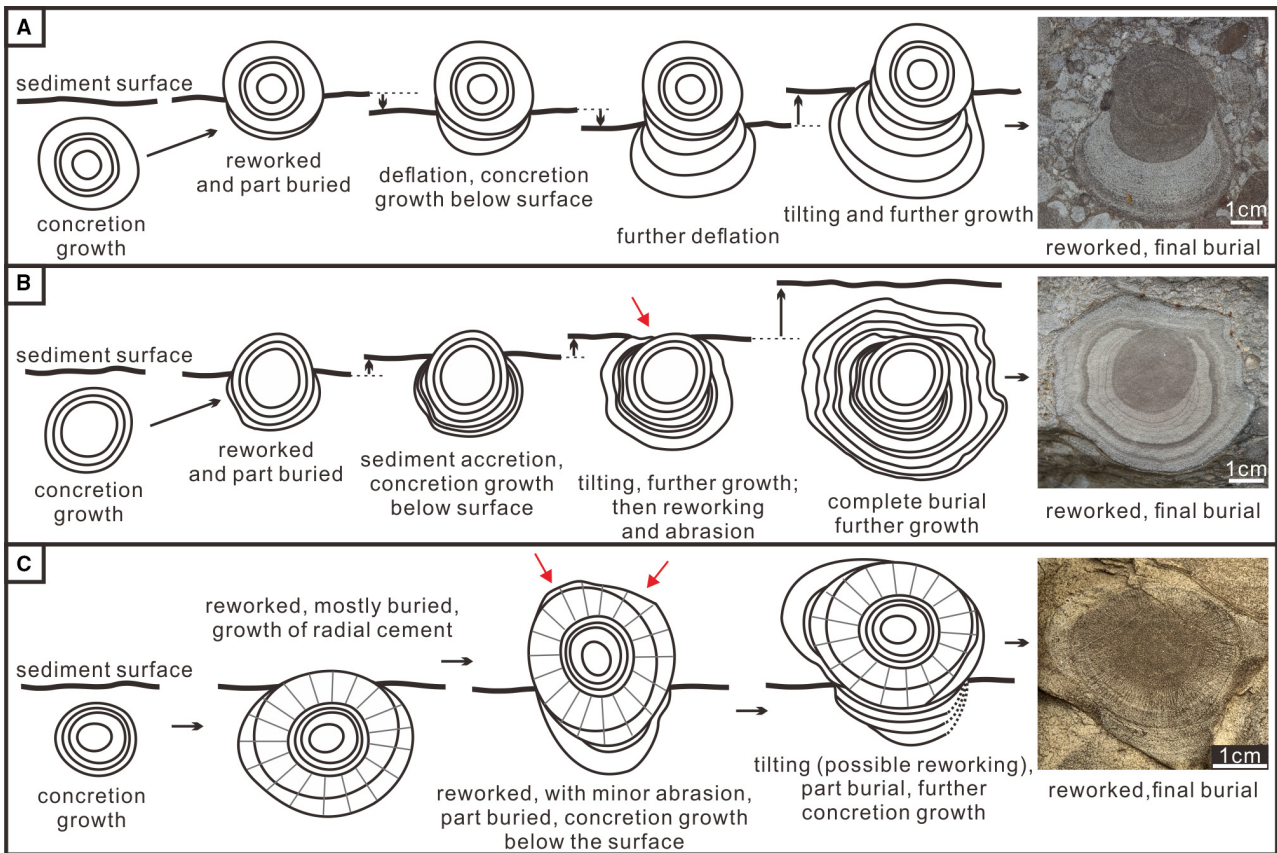
Fig. 13. Interpreted history of growth of three concentrically-laminated concretions (CLCs), showing phases of cement growth immediately below the sediment surface, punctuated by reorientation, reworking and abrasion (red arrows) episodes. (A) Asymmetrical concretion with pendulous growth. (B) Near-symmetrical concretion with phase of erosive truncation. (C) Concretion showing a phase of radially-oriented calcite crystal growth and phases of growth where only the lowermost surface of the CLC saw concretion growth.

Fig. 14. (A) Intraclast conglomerate beds with large sandstone/amalgamated clasts and concentrically-laminated concretions (CLCs). The dashed line in (A) highlights a large intraclast of conglomerate reworked from an older conglomerate bed. (B) Conglomerate bed with a single limestone clast in the upper right. Both from Yuntouling.

suggesting that they have been transported into the depositional environment, although it is possible that they are derived from rare beds encountered within the Liujiagou environment which were not observed during our study.
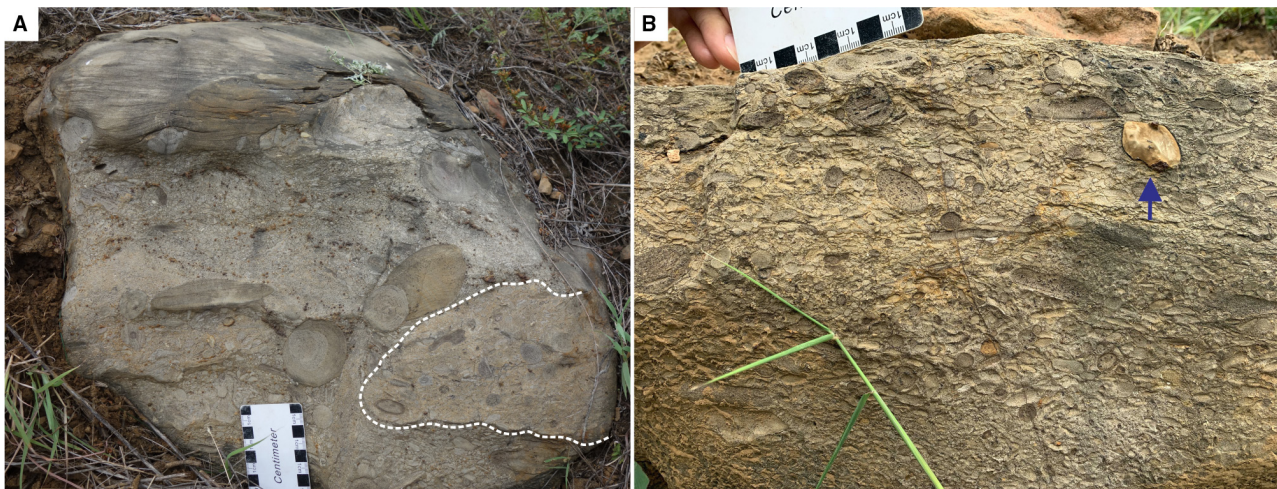
ORIGIN OF INTRACLAST CONGLOMERATES

The conglomerates of the Liujiagou Formation clearly record powerful erosive events that cannibalized older conglomerate horizons and exhumed and transported sandstone intraclasts and concretions up to the size of boulders. The largest clasts are angular and appear to have been derived by the fragmentation of a lithified lake bed, something that would have required exceptional energy. Inverse grading, where present, occurs as a result of larger particles moving away from the bed, through a geometrical mechanism of larger particles moving over smaller ones, and kinetic sieving as smaller particles move downward (Sohn, 1997; Dasgupta & Manna, 2011). Powerful, storm-generated waves were likely initially responsible for the generation of clasts, by brecciation and deflation of the lake bed, and then for providing the turbulent dispersion necessary to move the largest clasts up to mid-flow levels (Fig. 15). However, the local presence of imbrication near the base of some beds suggests intergranular collisions and laminar flow in the final stage of clast deposition (cf. Walker, 1975).

The vertical alignment of flat pebbles in the uppermost parts of conglomeratic beds is highly

A

Pre-event: extensive, cementation occurring in sand and gravel beds, including growth of CLC.

B

Early phase: powerful storm waves loading fragments lithified substrate, exhumes CLC.

C

Mid-phase: wave-influenced, sediment-gravity, current moves offshore, shearing generates imbrication of flat pebbles. Sand in suspension.

D

Late stage: Sand settles from suspension and infiltrates conglomerate matrix. Oscillatory flow reorientates clasts in the top of the bed.

- ◎ CLC
- ➤ flat pebble
- ● cemented patch
- ● compound intraclast
- → oscillatory flow
- → vertical settling
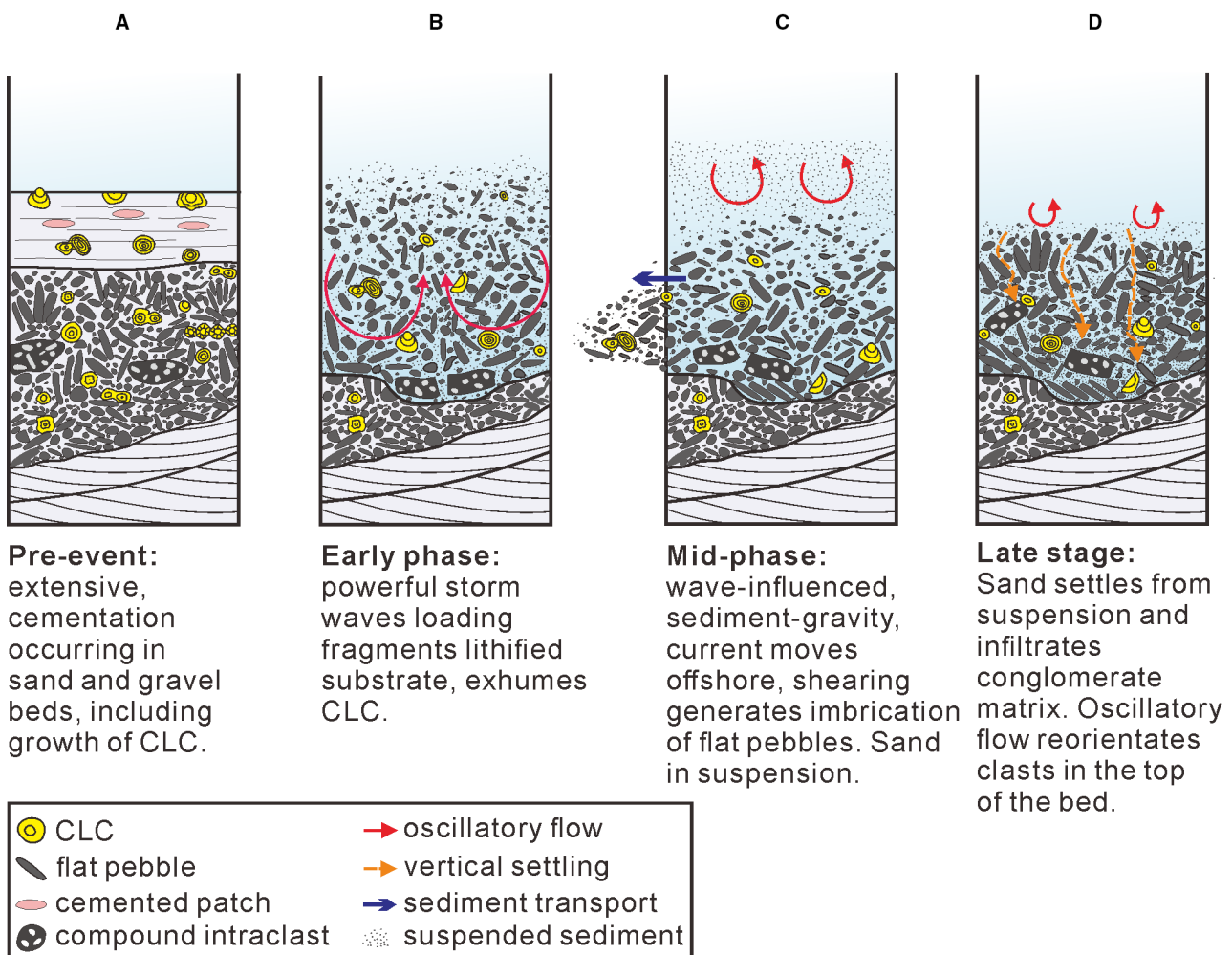- → sediment transport
- ∷ suspended sediment

Fig. 15. Four-stage model for the generation of intraclast conglomerates in the Liujiagou Formation.

unusual and unlikely to have occurred intrinsically in a high-density flow. This recalls the vertical stacking of shells seen in wave-agitated settings today (Sanderson & Donovan, 1974) and is also seen in flat pebble conglomerates attributed to storm events (Wignall & Twitchett, 1999), where rosettes also occur (Myrow *et al.*, 2004). The vertical alignment suggests that the final stages of conglomerate emplacement saw lateral flow cease but orbital water movement was still present and able to orientate the flat pebbles. Thus, oscillatory flow may have been acting throughout the history of bed formation, initially eroding the substrate, then maintaining turbulence during flow of a high-concentration sediment-gravity current, and finally reworking the flat clasts in the top of the bed once flow had ceased (Fig. 15). Suspension of clasts by oscillatory currents would probably have been necessary to generate the sediment-gravity flow because depositional gradients on the lake bed were likely very low. Wave modification of sediment-gravity currents has also been invoked to explain the origin of shoreline and shelf turbidites in low-gradient marine settings (Myrow *et al.*, 2002; Lamb *et al.*, 2008). The presence of shelter porosity and the development of a sand matrix in the lower parts of conglomerate beds suggests that sand settled vertically through the pore spaces of the bed after the coarser material accumulated. This could have occurred in the latest stages of a waning flow as sand, transported in suspension, settled into the open pores of the conglomerate.

The high-concentration sediment gravity flows were likely non-cohesive debris flows (*sensu* Talling *et al.*, 2012). Clasts do not project above the bed tops, indicating that more cohesive-style flow did not occur. However, occasional cross-bedding developed both within the conglomerates and gradationally above the beds, in overlying sandstone, suggests that some flows occasionally evolved to lower concentrations that allowed bedform development.

DISCUSSION

The sedimentology of the Liujiagou Formation records a range of depositional environments located around fluvial systems and the transition into shallow lakes subject to fair-weather and storm waves. Additionally, this setting was subject to high-energy events that generated high concentration flows capable of transporting clasts up to boulder size. These flows were preceded by considerable deflation of the lake bed that exhumed concretions and fragmented cemented areas of substrate. Similar storm-wave fragmentation of lithified carbonate substrates has been recorded from marine settings (Bouchette *et al.*, 2001). Potentially such erosion and deposition events could record major flash floods into the lake environment following catastrophic rainfall in the hinterland. However, the conglomerate beds are almost entirely composed of clasts generated within the depositional environment indicating that they were not associated with an influx of material. Evidence for late stage oscillatory flow is also unlikely in a flash-flood scenario.

Storm sedimentation is well-known from large lake bodies, and generates characteristic facies such as hummocky cross-stratified sandstone (Greenwood & Sherman, 1986; Tänavsuu-Milkeviciene & Frederick Sarg, 2012; Schuster & Nutz, 2018; Zhang *et al.*, 2018). Coarser, storm-related facies are also known. In the modern Great Lakes, storms produce metre-deep scours filled with bedded gravel and coarse sand in shoreface settings (Bray & Carter, 1992). A local, intraformational beach rock conglomerate has been documented from a Late Triassic lake in south-west England (Milroy & Wright, 2000). This example is considered to have formed by *in situ* brecciation of lithified beds of oolite by storms that re-orientated and aligned the coarse clasts. Clearly, wave and storm energy can be considerable in large lakes and capable of eroding, winnowing and transporting coarse sediment. However, the North China Basin conglomerates record events of exceptional strength for a lacustrine setting, which were capable of generating and transporting much larger clasts than those reported from other lakes. The evidence for extremely powerful events raises the possibility that hurricanes may have been impacting the North China Basin in the Early Triassic. Modern hurricanes are capable of considerable substrate erosion but they tend to be associated with only modest lateral transport (especially when compared with major winter storms) because they do not couple effectively with the water column; their high speeds ensure that there is little time for this to occur (Duke, 1985), with the result that their deposits consist of remobilized local sediment (Goni *et al.*, 2007). This is seen with the Liujiagou conglomerates which were essentially generated *in situ* from the interbedded sediment (including the

reworking of earlier conglomerates) followed by transport and emplacement within the same sedimentary setting.

Oxygen isotope and earth-system modelling evidence indicates that ocean surface temperatures adjacent to the North China continent reached temperatures >35°C in the Early Triassic (Sun *et al.*, 2012; Penn *et al.*, 2018). This is likely to have intensified the monsoonal climate and generated hurricanes of immense power in the open ocean. However, hurricanes typically lose their energy on landfall and would not generally be expected to impinge upon lake systems. Nonetheless, hurricanes may have transited into the North China Basin lake because there was unlikely to have been a major terrestrial barrier between the Palaeo-Tethys Ocean to the south-west (Fig. 1). Marine fossils are intermittently encountered in this area, suggesting that there was little to hinder a hurricane's passage into the Basin where they could be sustained by latent energy from the lake. Hurricanes derive their energy from the upper ocean with the effect being weakened when surface temperatures are decreased by vertical, turbulent mixing of cooler deeper waters. Such an effect is not seen in broad, shelf seas and this helps to counterbalance the effect of the relatively low volume of warm waters in such shallow-water settings. As a consequence, some modern, shelf seas often see intensification of a hurricane's strength as they progress across them (Price, 2009). Furthermore, future warming conditions are predicted to see the rate of decay of hurricanes on landfall diminish considerably (Li & Chakraborty, 2020). In the super-greenhouse world of the Early Triassic the impact of hurricanes in continental settings could therefore have been considerable.

The frequency of the high-energy (hurricane?) events in the North China basins is difficult to assess but the multiple episodes of reworking recorded by many intraclasts suggests that they were not uncommon. The evidence is diverse and includes concretions showing multiple phases of reworking (for example, Fig. 13), reworked conglomerate clasts and the many intraclasts that show phases of cement growth followed by reworking and abrasion (Fig. 10). More traditional storm deposition, in the form of the SCS facies, could also record hurricane events. More indirectly, the presence of gutter marks recording different flow directions to the overlying beds (Fig. 6) suggests that some storm/hurricane events generated erosional bypass surfaces that otherwise left no record. These were only covered by deposition from later flows.

The possibility that hurricanes were impacting sedimentation in a North China lake provides an indirect clue of high temperatures in the Early Triassic. More direct evidence comes from the abundant evidence for rapid cementation. The coarse, poikilotopic, sparry cement of the conglomerates is typical of that from a freshwater phreatic setting. The presence of clasts of cemented conglomerate within younger conglomerates indicates that this cementation was occurring near the sediment surface whilst the growth of CLCs may even have been at the sediment surface (Fig. 13). It is noteworthy that similar CLCs also occur in the coeval strata of the Katberg Formation, South Africa (Johnson, 1989), although they have not undergone reworking in their fluvial setting and so lack the complex histories of growth–erosion–regrowth seen in the Liujiagou Formation. High temperatures may also explain why the lake was essentially devoid of life for much of its Early Triassic history. Only several escape traces are recorded in this study while a few ichnofossils, for example limulid trackways (Shu *et al.*, 2018) and *Skolithos linearis*, *S. verticalis* and *Palaeophycus* (Guo *et al.*, 2019), are reported from the Liujiagou Formation. Limulids are able to survive in a much broader range of conditions, including high temperatures, than most lacustrine taxa, although experimental work has shown that even they perish at temperatures >35°C (Ehlinger & Tankersley, 2004).

CONCLUSION

Large lakes can record storm activity with hummocky and swaley cross-stratified sandstone being the most common product, and examples are seen from the Early Triassic North China Basin of North China. These occur amongst lacustrine facies that are associated with fluvial or fluviodeltaic facies. Also present are erosive-based, clast-supported, coarse conglomerate beds. These are interpreted to be the product of exceptionally powerful, erosive events that likely record the passage of hurricanes across the lake. The clasts were sourced by erosion of the lake bed and include extraordinary, concentrically-laminated concretions that record multiple episodes of burial, cementation and reworking, together with pebbles, cobbles and boulders of calcite-cemented sandstone and intraclast conglomerate. Short distance transportation of this material was in non-

cohesive debris flows subject to oscillatory currents that reworked the upper part of beds into stacked, edgewise flat-pebble conglomerates.

The occurrence of these unusual, intraclast conglomerates is likely due to a series of factors related to the high prevailing temperatures in the region in the Early Triassic. Such warmth favoured rapid cementation of the lake bed and likely generated frequent, powerful hurricanes in the adjacent ocean, which were able to travel into the lake system causing considerable lake-floor erosion.

ACKNOWLEDGEMENTS

DATA AVAILABILITY STATEMENT

The materials or data that support the findings of this study are available from the corresponding author upon request.

REFERENCES

Allen, B.J., Wignall, P.B., Hill, D.J., Saupe, E.E. and Dunhill, A.M. (2020) The latitudinal diversity gradient of tetrapods across the Permo-Triassic mass extinction and recovery interval. *Pro. Biol. Sci.*, **287**, 20201125.

Baud, A., Richoz, S. and Pruss, S. (2007) The lower Triassic anachronistic carbonate facies in space and time. *Glob. Planet. Change*, **55**, 81–89.

Bouchette, F., Séguret, M. and Moussine-Pouchkine, A. (2001) Coarse carbonate breccias as a result of water-wave cyclic loading (uppermost Jurassic - South-East Basin, France). *Sedimentology*, **48**, 767–789.

Bray Jr, T.F. and Carter, C.H. (1992) Physical processes and sedimentary record of a modern, transgressive, lacustrine barrier island. *Mar. Geol.*, **105**, 155–168.

Chu, D., Grasby, S.E., Song, H., Corso, J.D., Wang, Y., Mather, T.A., Wu, Y., Song, H., Shu, W., Tong, J. and Wignall, P.B. (2020) Ecological disturbance in tropical peatlands prior to marine Permian-Triassic mass extinction. *Geology*, **48**, 288–292.

Chu, D., Tong, J., Song, H., Benton, M.J., Bottjer, D.J., Song, H. and Tian, L. (2015) Early Triassic wrinkle structures on land: stressed environments and oases for life. *Sci. Rep.*, **5**, 10109.

Chu, D., Tong, J., Bottjer, D.J., Song, H., Song, H., Benton, M.J., Tian, L. and Guo, W. (2017) Microbial mats in the terrestrial Lower Triassic of North China and implications for the Permian-Triassic mass extinction. *Palaeogeogr. Palaeoclimatol. Palaeoecol.*, **474**, 214–231.

Chu, D., Tong, J., Benton, M.J., Yu, J. and Huang, Y. (2019) Mixed continental-marine biotas following the Permian-Triassic mass extinction in South and North China. *Palaeogeogr Palaeoclimatol Palaeoecol*, **519**, 95–107.

Dasgupta, P. and Manna, P. (2011) Geometrical mechanism of inverse grading in grain-flow deposits. *Earth-Sci Rev.*, **104**, 186–198.

Duke, W.L. (1985) Hummocky cross-stratification, tropical hurricanes, and intense winter storms. *Sedimentology*, **32**, 167–194.

Ehlinger, G.S. and Tankersley, R.A. (2004) Survival and development of horseshoe crab (*Limulus polyphemus*) embryos and larvae in hypersaline conditions. *Biol. Bull.*, **206**, 87–94.

Fairchild, I.J., Frisia, S., Borsato, A. and Tooth, A.F. (2006) Speleothems. In: *Geochemical Sediments and Landscapes* (Eds Nash, D.J. and McLaren, S.J.). Blackwells, Oxford.

Fielding, C.R., Frank, T.D., McLoughlin, S., Vajda, V., Mays, C., Tevyaw, A.P., Winguth, A., Winguth, C., Nicoll, R.S. and Bocking, M.J. (2019) Age and pattern of the southern high-latitude continental end-Permian extinction constrained by multiproxy analysis. *Nat. Commun.*, **10**, 1–12.

Goni, M.A., Alleau, Y., Corbett, R., Walsh, J.P., Mallinson, D., Allison, M.A., Gordon, E., Petsch, S. and Dellapenna, T.M. (2007) The effects of Hurricanes Katrina and Rita on the seabed of the Louisiana shelf. *Sediment. Rec.*, **5**, 4–9.

Greenwood, B. and Sherman, D.J. (1986) Hummocky cross-stratification in the surf zone: flow parameters and bedding genesis. *Sedimentology*, **33**, 33–45.

Guo, W., Tong, J., Tian, L., Chu, D., Bottjer, D.J., Shu, W. and Ji, K. (2019) Secular variations of ichnofossils from the terrestrial Late Permian-Middle Triassic succession at the Shichuanhe section in Shaanxi Province, North China. *Glob. Planet. Change*, **181**, 102978.

Johnson, M.R. (1989) Paleogeographic significance of oriented calcareous concretions in the Triassic Katberg Formation, South Africa. *J. Sed. Petrol.*, **59**, 1008–1010.

Lamb, M., Myrow, P., Lukens, C., Houck, K. and Strauss, J. (2008) Deposits from wave-influenced turbidity currents: Pennsylvanian Minturn Formation, Colorado, USA. *J. Sediment. Res.*, **78**, 480–498.

Li, F., Gong, Q., Burne, R.V., Tang, H., Su, C., Zeng, K., Zhang, Y. and Tan, X. (2019) Ooid factories operating under hothouse conditions in the earliest Triassic of South China. *Glob. Planet. Change*, **172**, 336–354.

Li, L. and Chakraborty, P. (2020) Slower decay of landfalling hurricanes in a warmer world. *Nature*, **587**, 230–234.

Liu, Y.Q., Kuang, H.W., Peng, N., Xu, H., Zhang, P., Wang, N.S., An, W., Wang, Y., Liu, M. and Hu, X.F. (2015) Mesozoic basins and associated palaeogeographic evolution in North China. *J. Palaeogeogr.*, **4**, 189–202.

MacLeod, K.G., **Quinton, P.C.** and **Bassett, D.J.J.G.** (2017) Warming and increased aridity during the earliest Triassic in the Karoo Basin, South Africa. *Geology*, **45**, 483–486.

Milroy, P.G. and **Wright, V.P.** (2000) A highstand oolitic sequence and associated facies from a Late Triassic lake basin, south-west England. *Sedimentology*, **47**, 187–209.

Myrow, P.M., **Fischer, W.** and **Goodge, J.W.** (2002) Wave-modified turbidites: combined-flow shoreline and shelf deposits, Cambrian, Antarctica. *J. Sediment. Res.*, **72**, 641–656.

Myrow, P.M., **Tice, L.**, **Archuleta, B.**, **Clark, B.**, **Taylor, J.F.** and **Ripperdan, R.L.** (2004) Flat-pebble conglomerate: its multiple origins and relationship to metre-scale depositional cycles. *Sedimentology*, **51**, 973–996.

Penn, J.L., **Deutsch, C.**, **Payne, J.L.** and **Sperling, E.A.** (2018) Temperature-dependent hypoxia explains biogeography and severity of end-Permian marine mass extinction. *Science*, **362**, eaat1327.

Price, J. (2009) Metrics of hurricane-ocean interaction: vertically-integrated or vertically-averaged ocean temperature? *Ocean Sci.*, **5**, 351.

Pruss, S.B., **Corsetti, F.A.** and **Bottjer, D.J.** (2005) The unusual sedimentary rock record of the Early Triassic: a case study from the southwestern United States. *Palaeogeogr. Palaeoclimatol. Palaeoecol.*, **222**, 33–52.

Romano, M., **Bernardi, M.**, **Petti, F.M.**, **Rubidge, B.**, **Hancox, J.** and **Benton, M.J.** (2020) Early Triassic terrestrial tetrapod fauna: a review. *Earth-Sci. Rev.*, **210**, 103331.

Sanderson, D.J. and **Donovan, R.N.** (1974) The vertical packing of shells and stones on some recent beaches. *J. Sediment. Res.*, **44**, 680–688.

Schuster, M. and **Nutz, A.** (2018) Lacustrine wave-dominated clastic shorelines: modern to ancient littoral landforms and deposits from the Lake Turkana Basin (East African Rift System, Kenya). *J. Paleolimnol.*, **59**, 221–243.

Shu, W., **Tong, J.**, **Tian, L.**, **Benton, M.J.**, **Chu, D.**, **Yu, J.** and **Guo, W.** (2018) Limuloid trackways from Permian-Triassic continental successions of North China. *Palaeogeogr. Palaeoclimatol. Palaeoecol.*, **508**, 71–90.

Smith, R.M. and **Botha-Brink, J.** (2014) Anatomy of a mass extinction: sedimentological and taphonomic evidence for drought-induced die-offs at the Permo-Triassic boundary in the main Karoo Basin, South Africa. *Palaeogeogr. Palaeoclimatol. Palaeoecol.*, **396**, 99–118.

Sohn, Y.K. (1997) On traction carpet sedimentation. *J. Sed. Petrol.*, **67**, 502–509.

Sun, Y., **Joachimski, M.M.**, **Wignall, P.B.**, **Yan, C.**, **Chen, Y.**, **Jiang, H.**, **Wang, L.** and **Lai, X.** (2012) Lethally hot temperatures during the Early Triassic greenhouse. *Science*, **338**, 366–370.

Talling, P.J., **Masson, D.G.**, **Sumner, E.J.** and **Malgesini, G.** (2012) Subaqueous sediment density flows: Depositional processes and deposit types. *Sedimentology*, **59**, 1937–2003.

Tänavsuu-Milkeviciene, K. and **Frederick Sarg, J.** (2012) Evolution of an organic-rich lake basin–stratigraphy, climate and tectonics: Piceance Creek basin, Eocene Green River Formation. *Sedimentology*, **59**, 1735–1768.

Torsvik, T.H. and **Cocks, L.R.M.** (2016) *Earth history and palaeogeography*. Cambridge University Press, Cambridge, UK.

Tu, C., **Chen, Z.Q.**, **Retallack, G.J.**, **Huang, Y.** and **Fang, Y.** (2016) Proliferation of MISS-related microbial mats following the end-Permian mass extinction in terrestrial ecosystems: evidence from the Lower Triassic of the Yiyang area, Henan Province, North China. *Sediment. Geol.*, **333**, 50–69.

Walker, R.G. (1975) Generalized facies models for resedimented conglomerates of turbidite association. *Geol. Soc. Am. Bull.*, **86**, 737–748.

Wang, Z. and **Wang, L.** (1986) Late Permian fossil plants from the lower part of the Shiqianfeng (Shihchienfeng) Group in North China. *Bull. Tianjin. Inst. Geol. Min. Res*, **15**, 1–80.

Wignall, P.B. (2015) *The Worst of Times: How Life on Earth Survived Eighty Million Years of Extinctions*. Princeton University Press, Princeton, NJ.

Wignall, P.B. and **Twitchett, R.J.** (1999) Unusual intraclastic limestones in Lower Triassic carbonates and their bearing on the aftermath of the end-Permian mass extinction. *Sedimentology*, **46**, 303–316.

Woods, A.D., **Bottjer, D.J.** and **Corsetti, F.A.** (2007) Calcium carbonate seafloor precipitates from the outer shelf to slope facies of the Lower Triassic (Smithian-Spathian) Union Wash Formation, California, USA: Sedimentology and palaeobiologic significance. *Palaeogeogr. Palaeoclimatol. Palaeoecol.*, **252**, 281–290.

Zhang, C., **Wang, H.**, **Liao, J.**, **Liao, Y.**, **Wei, J.** and **Lu, Z.** (2018) Oligocene storm-induced lacustrine deposits in the Yaxi Area of the Jiuxi Basin, northeastern margin of the Tibetan Plateau. *J Asian Earth Sci.*, **161**, 122–138.

Zhu, Z., **Kuang, H.**, **Liu, Y.**, **Benton, M.J.**, **Newell, A.J.**, **Xu, H.**, **An, W.**, **Ji, S.**, **Xu, S.**, **Peng, N.** and **Zhai, Q.** (2020) Intensifying aeolian activity following the end-Permian mass extinction: Evidence from the Late Permian-Early Triassic terrestrial sedimentary record of the Ordos Basin, North China. *Sedimentolgy*, **67**, 2691–2720.